Letter

Geometric effects induce anomalous size-dependent active transport in structured environments

Pooja Chopra, David Quint,* Ajay Gopinathan, and Bin Liu†
Department of Physics, University of California, 5200 North Lake Road, Merced, California 95343, USA

(Received 22 October 2020; accepted 22 June 2022; published 11 July 2022)

The variations of transport efficiency in structured environments between distinct individuals in actively self-propelled systems are both hard to study and poorly understood. Here, we study the transport of a nontumbling *Escherichia coli* strain, an active-matter archetype with intrinsic size variation but fairly uniform speed, through a periodic pillar array. We show that long-term transport switches from a trapping dominated state for shorter cells to a much more dispersive state for longer cells above a critical bacterial size set by the pillar array geometry. Using a combination of experiments and modeling, we show that this anomalous size dependence arises from an enhancement of the escape rate from trapping for longer cells caused by nearby pillars. Our results show that geometric effects can lead to size being a sensitive tuning knob for transport in structured environments, with implications in general for active matter systems and, in particular, for the morphological adaptation of bacteria to structured habitats, spatial structuring of communities, and for antibiofouling materials design.

DOI: 10.1103/PhysRevFluids.7.L071101

The structural features of environments have been recently shown to have a significant impact on the motility phases of active matter systems [1–12]. However, much less is known about how the interplay between variations in individual particle geometry and environmental structure affects macroscopic transport. For motile bacterial systems, in particular, such effects [13–17] can have implications for tunable transport in structured habitats. These implications arise because bacteria come in a variety of shapes and sizes across species [18–20] and even within a single strain [21–23]. It has been suggested that such widely distributed shapes and sizes are a consequence of adaptation to a diversity of features in their environments ranging from mechanical properties to nutrient availability [18]. In particular, the optimization of transport or dispersal is known to provide a strong selective pressure for bacterial morphology evolution [18,24–26]. For bacteria that live in structured or porous environments such as soil or tissue [27,28], proximity to a surface involves a whole host of physical interactions. These include hydrodynamic [29–32], electrostatic [33], and steric [34] forces as well as flow-induced effects [14,15,35], which could affect transport in a geometry-dependent manner [16,36,37]. Here,we study the possibility that the interplay between minor, intrinsic variations in the geometry of swimmers and structural features of the environment could lead to significant transport effects at the macroscopic scale.

One of the main challenges for such a study is that, in a standard microscope setting, a freely moving individual cell can only be observed, with the adequate resolution of individual geometry, over a length scale similar to that of the cell size ($\sim$10 μm). Meaningful statistics for its long-range

*Present address: Physical and Life Sciences, Lawrence Livermore National Laboratory, 7000 East Avenue, Livermore, California 94550, USA.
†bliu27@ucmerced.edu

 ©2022 American Physical Society

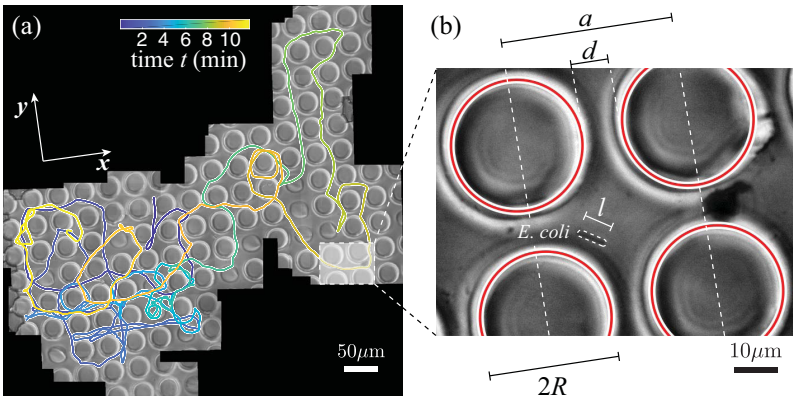

FIG. 1. Simultaneous large-scale and high-resolution study of bacterial transport in a micropillar array through active tracking and image stitching. (a) The trajectory of a single *E. coli* (tracked up to ∼1 mm in distance and ∼10 min in time) was reconstructed to characterize its long-term transport. The trajectory is color coded in time. (b) The high resolution that was preserved in each original frame in (a) provided the detailed cell and pillar geometry. The pillars were $R = 15$ μm in radius, arranged in a square lattice with a lattice constant of $a = 40$ μm, and a gap of $d = a - 2R = 10$ μm between adjacent pillars. The tracked bacterium (in a dashed contour) was $l \approx 6$ μm in length.

transport over the millimeter scale is therefore hard to obtain. Here, we resolved this issue by following individual bacteria via a tracking microscope, where the microscope stage is adjusted in real time to recenter the cell of interest in the field of view [25]. To provide a structured environment, we fabricated a rectangular microfluidic channel, 1 mm wide and 30 μm deep, embedded with square arrays of micropillars using a standard soft photolithography method. A typical pillar array with pillar radii $R = 15$ μm and lattice size $a = 40$ μm (with the closest gap thus $d = a - 2R = 10$ μm) is shown in Fig. 1(a). To focus on purely geometrical effects on transport that are applicable to generic active matter systems, we used a smooth swimming *Escherichia coli* strain, HCB437, which avoids any potential active response by the bacteria switching between run and tumble phases [38]. Additionally, this strain shows a natural length variation from 2 to 10 μm between individuals allowing us to examine the effects of microscopic geometry on macroscopic transport. We visualized the transport of these bacteria through the pillar array at a high (60× or 100×) magnification over millimeters by reconstructing trajectories. This was done by stitching together single image frames during the course of tracking (see Supplemental Material [39]) as shown in Fig. 1(b). Even though the tracked bacterium navigates the pillar array over a long distance, its detailed movement and orientation can still be resolved by visiting every single frame with a submicron resolution [Fig. 1(b)].

We first examined in detail the trajectories of several bacteria with different sizes. Independent of size, bacteria are constrained to move within the open spaces between pillars and the presence of noise leads to an overall diffusive trajectory at long times. However, we noticed two qualitatively different modes of motility depending on size. Short cells (2–5 μm), on the one hand, frequent the pillar surfaces and move mostly in circular patterns, due to effective hydrodynamic trapping [30,32,36] by the pillar array [Fig. 2(a); also see Movie S1 [39]]. Distinct from a plane-wall-induced circulation [29], this circulation around the pillar is bidirectional, regardless of the chirality embedded in the flagellar filaments (Supplemental Material Fig. S7 [39]). Longer cells, on the other hand, appear to escape from such traps, resulting in more persistent movement along the directions of two orthogonal lattice vectors (here, x and y axes) [Fig. 2(a); also see Movie S2 [39]]. Thus, longer cells, despite feeling an increased confinement, showed an anomalous increase in their net transport.

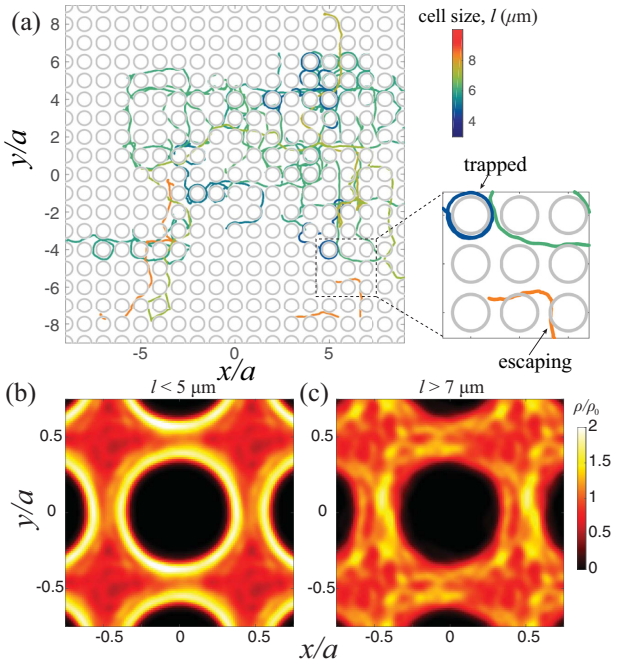

FIG. 2. Cell size-dependent trapping and escaping effects. (a) Multiple trajectories for different individuals (color coded by cell length l) are mapped to the same pillar array. The shorter cells tend to circulate around the pillars while the longer cells tend to navigate between the pillars, indicating the distinct trapped and escaping mechanisms, respectively (highlighted in the inset). (b) Probability distribution ρ of the shorter cells ($l < 5$ μm), normalized by a uniform density ρ_0, shows an effective enhancement at the pillar surface. (c) A similar plot for longer cells ($l > 7$ μm) shows the opposite effect.

To further quantify these distinct effects of the pillar array on bacteria with different sizes, we computed the probability distribution of the centers of bacteria in space within a single unit cell. As shown in Figs. 2(b) and 2(c), shorter bacteria are concentrated near the pillar surface (consistent with a hydrodynamic attraction [14]), while longer cells spend more time in the channels, confirming a size-dependent trapping effect. It is worth noting that tracking the front end of a cell provides essentially the same distribution near the pillar surface (Supplemental Material Fig. S5 [39]), suggesting a negligible role of cell length in volume exclusion.

To understand the mechanism governing this effect, we considered the geometric constraints on a swimming bacterium due to neighboring pillars. For simplicity, the bacterium is regarded as a rod-shaped pusher of length l_p, which is the effective hydrodynamic size set by the flow profile of the entire swimmer including the cell body (of length l) and the flagella [Fig. 3(a) inset]. Such a pusher tends to circulate around a single pillar in its natural state (without any neighboring pillars), due to the known hydrodynamic attraction between a solid surface and a generic pusher swimmer, including both bacteria and synthetic microswimmers [37,40]. In the presence of the neighboring pillars, the allowable pusher sizes are restricted, with the maximum length $l_{p,\max}$ determined by the geometry [Fig. 3(a)]. In addition to the length constraint, a pusher is also subjected to hydrodynamic interactions from the neighboring pillars. Here, we consider a pusher circulating in the counterclockwise direction and assume the pusher's orientation is always tangential to the pillar surface that it is circulating around. Depending on the orientation of the pusher relative to the pillar lattice (denoted by angle γ), the pusher may experience a torque from the nearest-neighbor pillar that either promotes or inhibits its circulation around the pillar. Such distinct effects are determined by the orientation angle θ_p of the pusher relative to the surface normal of the nearest-neighbor

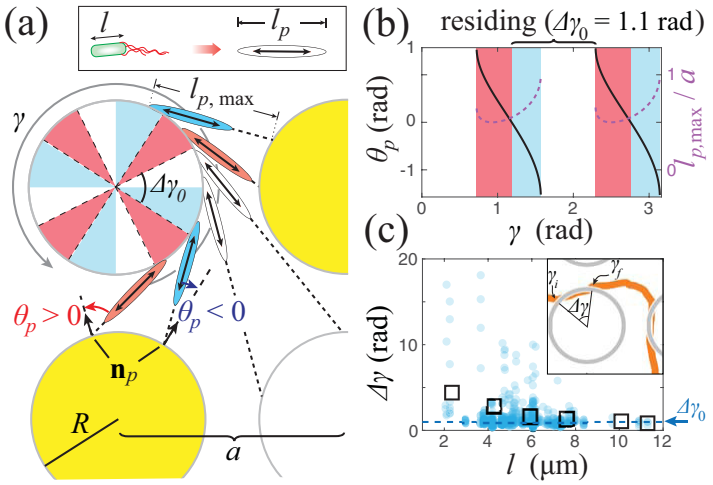

FIG. 3. Lattice-constrained bacterial residency on the pillar surface. (a) A "pusher" representation of the bacterium (inset, with a cell body length l and a total pusher length l_p) illustrates the geometric constraints for a bacterium circulating around a pillar (at angular position γ). An elongation of l_p to $l_{p,\max}$ (the greatest possible l_p without intersecting neighboring pillars) shows that the adjacent pillar (yellow) can either provide a positive (blue) or a negative (red) contribution to the circulation, demarcated by the orientation (θ_p) of the pusher relative to surface normal of a neighboring pillar $\mathbf{n}_p$. This leads to periodically attractive ($\theta_p < 0$ or without adjacent neighbors; blue or white) and repulsive ($\theta_p > 0$; red) zones on a pillar. (b) A computation of θ_p (solid lines) and maximum $l_{p,\max}$ (dashed lines) give rise to a residency arc angle $\Delta\gamma_0 = 1.1$ rad (for $a = 40$ μm, $R = 15$ μm). (c) The residency arc angles $\Delta\gamma$ (squares), averaged over individual residency events (solid circles), decrease with increasing l and eventually to values below the size of the attractive zone γ_0 (when $l \gtrsim 10$ μm), confirming suppressed circulation for longer cells.

pillar [Fig. 3(a)]. Here, we consider only the normal component of the hydrodynamic force from the pillar, associated with the anisotropic drag coefficients in the presence of a nearby wall [29,41]. For $\theta_p < 0$, the normal force from the nearest-neighbor pillar provides a torque that tends to tip the pusher toward the center of the pillar it is circulating around, leading to an effective attraction to the pillar surface. For $\theta_p > 0$, the torque due to the nearest-neighbor pillar tends to tip the pusher further away from the center causing the pusher to escape (likely along the tangent to the pillar surface). Considering the tangential components of the forces does not alter the directions of these torques, as long as the drag coefficient normal to the pillar surface dominates. It should be noted that we only treated the above pusher in a resistive-force-type manner to signify the geometric roles played by the nearest-neighbor pillar. More qualitative and quantitative insights of the hydrodynamic interactions requires resolving the flow field associated with a full pusher model including no-slip boundaries with pillar geometries [30].

This nearest-neighbor effect leads to a series of alternating attractive and repulsive zones along the perimeter of the pillar [with $\gamma \in [0, 2\pi)$], determined by the sign of θ_p. Figure 3(b) shows the calculated θ_p and $l_{p,\max}$ (see Supplemental Material [39]) for a counterclockwise circulating pusher and a pillar lattice that is consistent with the experimental setting ($R/a = 0.375$). The attractive ($\theta_p < 0$) and repulsive ($\theta_p > 0$) zones are shaded in red and blue, respectively. Zones that lack any constraints from the nearest-neighbor pillar (in white) are also considered attractive, due to the natural circulating state of pushers (in the absence of the neighboring pillars). This result shows four continuous attractive zones (blue plus white) along the perimeter of the pillar, with each spanning an arc angle $\Delta\gamma_0 = 1.1$ rad, centered near $\gamma = 0, \pi/2, \pi$, and $3\pi/2$, respectively.

To facilitate a more quantitative comparison between the experiment and the theoretical picture, we measured a residency arc angle $\Delta\gamma = \gamma_f - \gamma_i$, which is the difference between the two angles

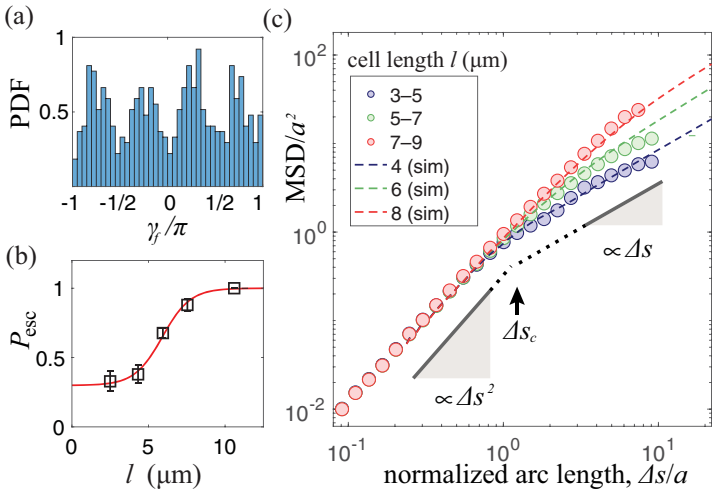

FIG. 4. Size-dependent escaping and global diffusivity. (a) The nonuniform distribution of angles of escaping [γ_f, illustrated in Fig. 3(c) inset] shows more probable escaping of bacteria along the diagonals (i.e., $k\pi/4$ with $k = \pm 1, \pm 3$) of the square lattice, consistent with the locations of the repulsive zones. (b) The escaping probabilities P_{esc} are calculated from bacterial trajectories for different cell lengths l (open squares with error bars representing the standard errors). The solid curve corresponds to a fit with a hyperbolic tangent function. (c) The mean-squared displacement (MSD) as a function of the path length (Δs) exhibits a transition from a ballistic regime (MSD $\propto \Delta s^2$) to a diffusive one (MSD $\propto \Delta s$) for both experiments (circles) and numerical simulations (see Supplemental Material) with the corresponding P_{esc} (dashed lines). The size of the ballistic regimes, depicted by a ballistic length Δs_c (arrow), increase with l or P_{esc}, consistent with the geometry-induced escaping for longer cells. All lengths in trajectories are normalized by lattice size a.

where the bacterium enters (γ_i) and escapes (γ_f) the vicinity of the pillar surface [Fig. 3(c) inset]. The bacteria continuously circulate the pillar over an arc subtending this angle without leaving the surface. The experimental residency arc angles $\Delta\gamma$, plotted against cell lengths l, are shown in Fig. 3(c). At short cell lengths ($l \lesssim 4$ μm), $\Delta\gamma$ can span over larger angles ($\Delta\gamma > 2\pi$), corresponding to the presence of multiturn circulations. As l increases, $\Delta\gamma$ becomes restricted only to small angles (e.g., $\Delta\gamma \lesssim \pi$ for $l \gtrsim 7$ μm). Such a restriction in the distribution of $\Delta\gamma$ is responsible for the decrease in its mean with increasing l. For sufficiently long l ($l \gtrsim 10$ μm), the mean $\Delta\gamma$ falls beneath the size of the computed attractive zone ($\Delta\gamma_0 = 1.1$ rad), consistent with a highly constrained pusher that is unable to bypass any repulsive zones (as required for circulations beyond a single attractive zone). We also note that there is no such size dependence of $\Delta\gamma$ for sufficiently large gaps among pillars (Supplemental Material Fig. S6 [39]), which further validates our geometric arguments.

To further validate our model, we investigated the statistics of the angles γ_f at which bacteria escaped the pillar surface. The probability density function (PDF) of γ_f shows peaks near the diagonal directions of the pillar lattice [Fig. 4(a)], consistent with the predicted locations of the repulsive zones [Fig. 3(b)]. This highly anisotropic distribution of γ_f also justifies the use of a single escaping probability P_{esc} (within all repulsive zones only) for characterizing the size-dependent geometric effects. Such an escaping probability is consistent with the stochastic nature of the competition between both the hydrodynamic attraction from the orbited pillar and the "repulsive" contribution from the nearest-neighboring one, associated with the fluctuating orientation and location of a microswimmer. If we consider that bacteria only escape within repulsive zones, P_{esc} can be obtained as $P_{esc} = \frac{N_e}{N_z}$, where N_e and N_z correspond respectively to the number of escaping events and the number of repulsive zones that bacteria cross during their travel along the pillars' perimeters.

Noting that the angular separation between the centers of two adjacent repulsive zones is $\pi/2$ and neglecting the detailed escaping locations, the number N_z is given by $N_z = \sum_{i=1}^{N_e}([2\Delta\gamma_i/\pi] + 1)$, where i corresponds to the index of an escaping event and $[\cdot]$ denotes the integer part of a number. The escaping probability is thus the inverse of an ensemble average (denoted by $\langle\cdot\rangle$), i.e., $P_{\rm esc} = \langle[2\Delta\gamma/\pi + 1]\rangle^{-1}$. We computed this probability $P_{\rm esc}$ from experiments for different groups of cell body lengths l. As shown in Fig. 4(b), there is a transition from a low escaping probability ($P_{\rm exc} \approx 0.3$) for relatively shorter cells ($l \lesssim 5$ μm) to a high escaping probability ($P_{\rm exc} \approx 1$) for relatively longer ones ($l \gtrsim 7$ μm). A hyperbolic-tangent fit of the experimental data yields a function [solid curve in Fig. 4(b)] $P_{\rm esc}(l) = P_0 + (1 - P_0)\tanh[(l - l_c)/\Delta l]$ with the critical cell body length $l_c = 6.0$ μm demarcating the distinct escaping behaviors.

To show how this geometric effect manifests itself in the long-time transport of bacteria, we simulated bacterial trajectories by a kinematic model [using the above $P_{\rm esc}(l)$]: A bacterium that reaches a pillar surface stays on the surface and continues circulating the pillar if it is within an attractive zone or it escapes with a probability $P_{\rm esc}$ if it enters a repulsive zone [in red in Fig. 3(b)]. Here, we assumed that a bacterium moves at a constant speed u, which is a fairly good approximation for the nontumbling mutant (Supplemental Material Fig. S8 [39]). After escaping along the direction tangential to the pillar's circumference, the bacterium moves at constant speed until it reaches an attractive or repulsive zone of the next pillar along its trajectory. A white noise in the swimming direction was extracted from experimental trajectories (Supplemental Material Fig. S2 [39]) and introduced to the model swimmer when it is away from the pillar surface. We then computed the corresponding mean-squared displacement (MSD) for comparison with the experimental data [Fig. 4(c)]. To secure optimal convergence, the MSD values were binned by path lengths Δs and sampled over all trajectories within the same size l group. For all experimental MSD [dots in Fig. 4(c)], cell body lengths l (3–9 μm) were grouped every 2 μm to secure a sufficient number ($\gtrsim$20) of long trajectories ($\gtrsim$200 μm) within each size category. All data points with less than ten sampled trajectories were excluded. Each simulated MSD of the corresponding l [dashed line in Fig. 4(c)] was computed over 100 model swimmers with each of them traveling $400a$ in total path length s from a random starting position. As shown in Fig. 4(c), the simulated MSD reproduces well the characteristics of bacterial transport. In both experimental and simulated results, each MSD-Δs curve contains a ballistic regime for small Δs and a diffusive regime for large Δs. The size of the ballistic regime can be characterized by a ballistic length Δs_c [Fig. 4(c)], set by the crossover point between two distinct scaling regimes for transport (with MSD exponents $\alpha = 1$ and $\alpha = 2$). Interestingly, the ballistic length $\Delta s_c/a \approx 1$ for relatively shorter cells, reminiscent of the effective reorientation timescale $\tau = a/u$ for pointlike particles diffusing in obstacle networks [42,43]. While converging at short Δs, the long-time MSD-Δs curves are noticeably higher for longer cells, corresponding to longer ballistic lengths Δs_c at longer cell lengths l and thus suggesting a finite-length effect. Again, longer cells, despite feeling an increased confinement, display an anomalous increase in their MSD due to the geometric effects of the neighboring pillars. These quantitative agreements between the experiment and theory further confirm the dominant role played by geometry.

Our study illustrates the role of individual morphology in the transport of active particles in general and bacteria, in particular, through periodic structured media. In living systems, this surprising enhancement of transport for longer cells, combined with a maximal cell size set by interstitial spaces of the lattice, suggests an optimal cell size potentially determined by the geometry of a porous environment [18,24,44]. Similar geometry-sensitive effects in the transport of wild-type strains may already be present, but not explicitly identified, in other studies of bacterial transport [17]. Generalizing our geometric effects to such three-dimensional (3D) environments will enable the targeted design of environmental geometry for desired size-dependent transport and collective motion [13,45,46]. For a nonperiodic lattice, it is expected that the above geometric effect still applies in general, since any geometric constraints due to nearest-neighbor pillars always tend to influence the longer cells first before they can influence shorter cells. However, the location and size

of the repulsive zones, as well as the critical cell-body length, now vary for each pillar, leading to more complex escaping zones and thus more complex global cell kinematics. Also, in the extreme case that multiple pillars are within the vicinity, a long cell will be more easily jammed as it requires more room for reorientation, contributing to another type of geometric constraint. These potential effects due to disorder in the crystalline structure of the environment will be investigated in our future work.

Our findings also indicate that the transition between localized and dispersive modes is sharp and occurs at a critical value of bacterial size, controlled by the porous environment. Bacteria with typical sizes near this critical value may be able to access both modes of transport by adaptive change in their size based on the local nutrient conditions or other desired transport needs. This suggests, for example, an unexplored benefit of filamentation under starvation conditions in *E. coli*, in addition to others that have been proposed in the literature [47–49]. Our results also have implications for the spatial structure of naturally occurring bacterial colonies in structured environments where spatial location within the colony could be correlated with age-dependent cell size, due to differential transport.

In nature, patterned structures with periodic lattices are widely found on antibiofouling surfaces, such as cicada wings [50] and shark skins [51]. The geometric effects we have identified thus provide another perspective for revisiting these microscale structures in relation to their antibiofouling effects. Conversely, our work also suggests ways to engineer surfaces so as to either increase or decrease the residency of different bacterial strains with slightly different sizes or even differentiating age structured populations, which may also be of interest in biofouling applications. Such ideas could also be applied to designing environments for the desired sorting or guiding of synthetic microswimmers as well as the geometric design of individual swimmers.

We would like to thank Howard Berg for providing the *E. coli* mutant strain used in this study. We also acknowledge Jeremias Gonzalez, Yu Zeng, and Jacinta Conrad for insightful discussions and the Stem Cell Instrumentation Foundry at UC Merced for using the microfabrication facility. This work was supported by National Science Foundation Grants No. CBET-2046822 and No. CBET-1706511, and NSF-CREST: Center for Cellular and Bio-molecular Machines (CCBM) at UC Merced (HRD-1547848 and HRD-2112675). B.L. is thankful for the support of the Hellman Foundation. A.G. also acknowledges support from National Science Foundation (NSF) Grant No. DMS-1616926, partial support from the NSF Center for Engineering Mechanobiology Grant No. NSF CMMI-154857, and the hospitality of the Aspen Center for Physics, which is supported by NSF Grant No. PHY-1607611.

[1] C. Bechinger, R. Di Leonardo, H. Löwen, C. Reichhardt, G. Volpe, and G. Volpe, Active particles in complex and crowded environments, Rev. Mod. Phys. **88**, 045006 (2016).

[2] A. Morin, N. Desreumaux, J.-B. Caussin, and D. Bartolo, Distortion and destruction of colloidal flocks in disordered environments, Nat. Phys. **13**, 63 (2017).

[3] D. A. Quint and A. Gopinathan, Topologically induced swarming phase transition on a 2D percolated lattice, Phys. Biol. **12**, 046008 (2015).

[4] O. Chepizhko and F. Peruani, Diffusion, Subdiffusion, and Trapping of Active Particles in Heterogeneous Media, Phys. Rev. Lett. **111**, 160604 (2013).

[5] T. Bertrand, Y. Zhao, O. Bénichou, J. Tailleur, and R. Voituriez, Optimized Diffusion of Run-and-Tumble Particles in Crowded Environments, Phys. Rev. Lett. **120**, 198103 (2018).

[6] Cs. Sándor, A. Libál, C. Reichhardt, and C. J. Olson Reichhardt, Dynamic phases of active matter systems with quenched disorder, Phys. Rev. E **95**, 032606 (2017).

[7] S. Pattanayak, R. Das, M. Kumar, and S. Mishra, Enhanced dynamics of active Brownian particles in periodic obstacle arrays and corrugated channels, Eur. Phys. J. E **42**, 62 (2019).

[8] T. V. Phan, R. Morris, M. E. Black, T. K. Do, K.-C. Lin, K. Nagy, J. C. Sturm, J. Bos, and R. H. Austin, Bacterial Route Finding and Collective Escape in Mazes and Fractals, Phys. Rev. X **10**, 031017 (2020).
[9] H. E. Ribeiro, W. P. Ferreira, and F. Q. Potiguar, Trapping and sorting of active matter in a periodic background potential, Phys. Rev. E **101**, 032126 (2020).
[10] S. Yazdi, J. L. Aragones, J. Coulter, and A. Alexander-Katz, Metamaterials for active colloid transport, arXiv:2002.06477.
[11] M. Brun-Cosme-Bruny, A. Förtsch, W. Zimmermann, E. Bertin, P. Peyla, and S. Rafaï, Deflection of phototactic microswimmers through obstacle arrays, Phys. Rev. Fluids **5**, 093302 (2020).
[12] C. Reichhardt and C. J. O. Reichhardt, Directional locking effects for active matter particles coupled to a periodic substrate, Phys. Rev. E **102**, 042616 (2020).
[13] H. Wioland, F. G. Woodhouse, J. Dunkel, and R. E. Goldstein, Ferromagnetic and antiferromagnetic order in bacterial vortex lattices, Nat. Phys. **12**, 341 (2016).
[14] A. Creppy, E. Clément, C. Douarche, M. V. D'Angelo, and H. Auradou, Effect of motility on the transport of bacteria populations through a porous medium, Phys. Rev. Fluids **4**, 013102 (2019).
[15] A. Dehkharghani, N. Waisbord, J. Dunkel, and J. S. Guasto, Bacterial scattering in microfluidic crystal flows reveals giant active Taylor–Aris dispersion, Proc. Natl. Acad. Sci. USA **116**, 11119 (2019).
[16] S. Makarchuk, V. C. Braz, N. A. M. Araújo, L. Ciric, and G. Volpe, Enhanced propagation of motile bacteria on surfaces due to forward scattering, Nat. Commun. **10**, 4110 (2019).
[17] T. Bhattacharjee and S. S. Datta, Bacterial hopping and trapping in porous media, Nat. Commun. **10**, 2075 (2019).
[18] K. D. Young, The selective value of bacterial shape, Microbiol. Mol. Biol. Rev. **70**, 660 (2006).
[19] M. S. Rappé, S. A. Connon, K. L. Vergin, and S. J. Giovannoni, Cultivation of the ubiquitous SAR11 marine bacterioplankton clade, Nature (London) **418**, 630 (2002).
[20] E. R. Angert, K. D. Clements, and N. R. Pace, The largest bacterium, Nature (London) **362**, 239 (1993).
[21] M. W. Hahn, E. R. Moore, and M. G. Höfle, Bacterial filament formation, a defense mechanism against flagellate grazing, is growth rate controlled in bacteria of different phyla, Appl. Environ. Microbiol. **65**, 25 (1999).
[22] A. Typas, M. Banzhaf, C. A. Gross, and W. Vollmer, From the regulation of peptidoglycan synthesis to bacterial growth and morphology, Nat. Rev. Microbiol. **10**, 123 (2012).
[23] J.-P. Shen, and C.-F. Chou, Morphological plasticity of bacteria—Open questions, Biomicrofluidics **10**, 031501 (2016).
[24] R. Schuech, T. Hoehfurtner, D. J. Smith, and S. Humphries, Motile curved bacteria are Pareto-optimal, Proc. Natl. Acad. Sci. USA **116**, 14440 (2019).
[25] B. Liu, M. Gulino, M. Morse, J. X. Tang, T. R. Powers, and K. S. Breuer, Helical motion of the cell body enhances *Caulobactercrescentus* motility, Proc. Natl. Acad. Sci. USA **111**, 11252 (2014).
[26] A. Persat, H. A. Stone, and Z. Gitai, The curved shape of *Caulobactercrescentus* enhances surface colonization in flow, Nat. Commun. **5**, 3824 (2014).
[27] G. A. Turnbull, J. W. Morgan, J. M. Whipps, and J. R. Saunders, The role of bacterial motility in the survival and spread of *Pseudomonas fluorescens* in soil and in the attachment and colonisation of wheat roots, FEMS Microbiol. Ecol. **36**, 21 (2001).
[28] S. Balzan, C. de Almeida Quadros, R. de Cleva, B. Zilberstein, and I. Cecconello, Bacterial translocation: Overview of mechanisms and clinical impact, J. Gastroenterol. Hepatol. **22**, 464 (2007).
[29] E. Lauga, W. R. DiLuzio, G. M. Whitesides, and H. A. Stone, Swimming in circles: Motion of bacteria near solid boundaries, Biophys. J. **90**, 400 (2006).
[30] S. E. Spagnolie, G. R. Moreno-Flores, D. Bartolo, and E. Lauga, Geometric capture and escape of a microswimmer colliding with an obstacle, Soft Matter **11**, 3396 (2015).
[31] H. Shum, E. A. Gaffney, and D. J. Smith, Modelling bacterial behaviour close to a no-slip plane boundary: The influence of bacterial geometry, Proc. R. Soc. London, Ser. A **466**, 1725 (2010).
[32] O. Sipos, K. Nagy, R. Di Leonardo, and P. Galajda, Hydrodynamic Trapping of Swimming Bacteria by Convex Walls, Phys. Rev. Lett. **114**, 258104 (2015).
[33] M. Hermansson, The DLVO theory in microbial adhesion, Colloids Surf., B **14**, 105 (1999).

[34] K. Drescher, J. Dunkel, L. H. Cisneros, S. Ganguly, and R. E. Goldstein, Fluid dynamics and noise in bacterial cell-cell and cell-surface scattering, Proc. Natl. Acad. Sci. USA **108**, 10940 (2011).
[35] R. Alonso-Matilla, B. Chakrabarti, and D. Saintillan, Transport and dispersion of active particles in periodic porous media, Phys. Rev. Fluids **4**, 043101 (2019).
[36] J. Tong and M. J. Shelley, Directed migration of microscale swimmers by an array of shaped obstacles: Modeling and shape optimization, SIAM J. Appl. Math. **78**, 2370 (2018).
[37] M. S. Davies Wykes, X. Zhong, J. Tong, T. Adachi, Y. Liu, L. Ristroph, M. D. Ward, M. J. Shelley, and J. Zhang, Guiding microscale swimmers using teardrop-shaped posts, Soft Matter **13**, 4681 (2017).
[38] *E. coli in Motion*, edited by H. C. Berg (Springer, New York, 2004).
[39] See Supplemental Material at http://link.aps.org/supplemental/10.1103/PhysRevFluids.7.L071101 for extra data and detailed methods.
[40] A. P. Berke, L. Turner, H. C. Berg, and E. Lauga, Hydrodynamic Attraction of Swimming Microorganisms by Surfaces, Phys. Rev. Lett. **101**, 038102 (2008).
[41] H. Brenner, The slow motion of a sphere through a viscous fluid towards a plane surface, Chem. Eng. Sci. **16**, 242 (1961).
[42] T. Jakuszeit, O. A. Croze, and S. Bell, Diffusion of active particles in a complex environment: Role of surface scattering, Phys. Rev. E **99**, 012610 (2019).
[43] K. Schakenraad, L. Ravazzano, N. Sarkar, J. A. J. Wondergem, R. M. H. Merks, and L. Giomi, Topotaxis of active Brownian particles, Phys. Rev. E **101**, 032602 (2020).
[44] L. R. Bakken and R. A. Olsen, The relationship between cell size and viability of soil bacteria, Microb. Ecol. **13**, 103 (1987).
[45] Z. Long, B. Quaife, H. Salman, and Z. N. Oltvai, Cell-cell communication enhances bacterial chemotaxis toward external attractants, Sci. Rep. **7**, 12855 (2017).
[46] D. Nishiguchi, I. S. Aranson, A. Snezhko, and A. Sokolov, Engineering bacterial vortex lattice via direct laser lithography, Nat. Commun. **9**, 4486 (2018).
[47] M. Wainwright, L. T. Canham, K. Al-Wajeeh, and C. L. Reeves, Morphological changes (including filamentation) in *Escherichia coli* grown under starvation conditions on silicon wafers and other surfaces, Lett. Appl. Microbiol. **29**, 224 (1999).
[48] C. Miller, L. E. Thomsen, C. Gaggero, R. Mosseri, H. Ingmer, and S. N. Cohen, SOS response induction by β-lactams and bacterial defense against antibiotic lethality, Science **305**, 1629 (2004).
[49] S. S. Justice, D. A. Hunstad, P. C. Seed, and S. J. Hultgren, Filamentation by *Escherichia coli* subverts innate defenses during urinary tract infection, Proc. Natl. Acad. Sci. USA **103**, 19884 (2006).
[50] E. P. Ivanova *et al.*, Natural bactericidal surfaces: mechanical rupture of *Pseudomonasaeruginosa* cells by cicada wings, Small **8**, 2489 (2012).
[51] J. F. Schumacher, M. L. Carman, T. G. Estes, A. W. Feinberg, L. H. Wilson, M. E. Callow, J. A. Callow, J. A. Finlay, and A. B. Brennan, Engineered antifouling microtopographies – effect of feature size, geometry, and roughness on settlement of zoospores of the green alga Ulva, Biofouling **23**, 55 (2007).